Journal of Magnetic Resonance **156,** 52–63 (2002)
doi:10.1006/jmre.2002.2527

Deconvolution of Compartmental Water Diffusion Coefficients in Yeast-Cell Suspensions Using Combined T_1 and Diffusion Measurements

Matthew D. Silva,* Karl G. Helmer,* Jing-Huei Lee,† Sam S. Han,* Charles S. Springer, Jr.,†,‡ and Christopher H. Sotak*,§,¶,[1]

*Department of Biomedical Engineering, Worcester Polytechnic Institute, Worcester, Massachusetts 01609; †Chemistry Department, Brookhaven National Laboratory, Upton, New York 11973; ‡Department of Chemistry, State University of New York, Stony Brook, New York 11794; §Department of Chemistry and Biochemistry, Worcester Polytechnic Institute, Worcester, Massachusetts 01609; and ¶Department of Radiology, The University of Massachusetts Medical School, Worcester, Massachusetts 01655

Received September 7, 2001; revised March 8, 2002; published online May 31, 2002

An NMR method is presented for measuring compartment-specific water diffusion coefficient (*D*) values. It uses relaxography, employing an extracellular contrast reagent (CR) to distinguish intracellular (IC) and extracellular (EC) ^1H_2O signals by differences in their respective longitudinal (T_1) relaxation times. A diffusion-weighted inversion-recovery spin-echo (DW-IRSE) pulse sequence was used to acquire IR data sets with systematically and independently varying inversion time (TI) and diffusion-attenuation gradient amplitude (*g*) values. Implementation of the DW-IRSE technique was demonstrated and validated using yeast cells suspended in 3 mM Gd-DTPA^{2-} with a wet/dry mass ratio of 3.25 : 1.0. Two-dimensional (2D) NMR data were acquired at 2.0 T and analyzed using numerical inverse Laplace transformation (2D- and sequential 1D-ILT) and sequential exponential fitting to yield T_1 and water *D* values. All three methods gave substantial agreement. Exponential fitting, deemed the most accurate and time efficient, yielded T_1 : *D* (relative contribution) values of 304 ms : 0.023 $\times$ 10^{-5} cm^2/s (47%) and 65 ms : 1.24 $\times$ 10^{-5} cm^2/s (53%) for the IC and EC components, respectively. The compartment-specific *D* values derived from direct biexponential fitting of diffusion-attenuation data were also in good agreement. Extension of the DW-IRSE method to *in vivo* models should provide valuable insights into compartment-specific water *D* changes in response to injury or disease. © 2002 Elsevier Science (USA)

Key Words: **relaxography; diffusigraphy; contrast reagent; yeast-cell suspension; water apparent diffusion coefficient.**

INTRODUCTION

Andrasko considered the idea that an NMR signal arising from biological tissue can be a mixture of signals from water or metabolite molecules exchanging between the intracellular (IC) and extracellular (EC) spaces (*1*). Therefore, the signal measured by standard NMR techniques may contain information that is weighted by NMR (e.g., relaxation times) and physical (e.g., diffusion coefficients) parameters of the two compartments. To better understand changes of these parameters in response to pathology, it would be useful to clearly separate and assign the contributions from each compartment, IC and EC, and determine if one or both are responsible for any overall NMR signal change.

Application of diffusion-weighted NMR techniques to *in vivo* systems was first demonstrated by Wesbey *et al*. (*2*) and Le Bihan *et al*. (*3*). Moseley *et al.* (*4*) demonstrated a decline in the apparent diffusion coefficient (ADC) of cerebral tissue water during ischemia, and this discovery has established ADC measurement as an effective technique for detecting acute stroke. However, the mechanism of this change is not yet fully understood. It is unclear whether the ischemic ADC decrease is related to changes in the IC space, EC space, or both. Previous studies have shown that water ADC changes in biological systems can result from changes in the cellular membrane permeability, relative changes in the volume fractions of the IC and EC spaces, or combinations of these (*5, 6*). Recent studies have also suggested that IC molecular diffusion in cerebral tissue also may be dependent on cytosolic streaming, an energy-dependent process that is retarded during ischemia (*7*). In order to provide additional insights into the mechanism of water ADC changes in response to ischemic injury, there is a pressing need for methodology that would provide compartment-specific information concerning water diffusion.

This paper presents an NMR method for measuring compartment-specific diffusion coefficients. It employs relaxography (*8, 9*), using a contrast reagent (CR) to distinguish between the IC and EC water proton signals based on differences in their respective longitudinal (T_1) relaxation times. This method is based on relaxography utilizing a numerical inverse Laplace transform (ILT) (*10–12*) of longitudinal relaxation data to produce a distribution of relaxation times that can be

[1] To whom correspondence should be addressed at Department of Biomedical Engineering, Worcester Polytechnic Institute, Worcester, MA 01609. E-mail: csotak@wpi.edu.

1090-7807/02 $35.00

multimodal, depending on the number of populations in the sample. If this so-called "relaxogram" displays two distinct relaxation time peaks, a discrete ILT regression converges on the continuous distribution means. Comparable results can also be obtained by fitting the data to a biexponential function using a constrained nonlinear least-squares algorithm (*9, 13, 14*). In this case, the biexponential model can accurately find the same distribution means that are derived from the relaxogram.

A diffusion analogue of relaxography (diffusigraphy (*15*)) can be performed by acquiring a series of diffusion-weighted NMR data while systematically varying values of the diffusion-weighting parameter (b value) defined below. The appropriate numerical ILT of such data can also produce a multimodal ADC distribution (a diffusigram (*15*)) that can facilitate discrimination of compartmental signals (*15, 16*). Alternatively, those data could also be subjected to discrete exponential analysis to extract the compartment-specific ADC values. The earlier 1D diffusigraphic results (*15*) were encouraging in that, at least for cell suspensions (*1, 15, 17*), the large ADC differences may be sufficient to allow discrimination without the necessity for CR. However, most intact tissue has a considerably higher cell density than can be generally achieved with suspensions of cells *in vitro* and thus is not likely to exhibit such large differences in diffusion coefficients. Consequently, an alternative approach is needed to quantify compartment-specific ADC values in cases where the respective compartmental ADC values may be similar.

Relaxography can be combined with other types of NMR measurements (e.g., image spatial encoding (*8*)) to acquire additional information from the separate compartmental signals. For the NMR method presented herein, relaxography is combined with diffusion encoding to measure compartment-specific ADC values from NMR signals that have been separated using CR-aided relaxography. The NMR method, based on a diffusion-weighted, inversion-recovery spin-echo (DW-IRSE) pulse sequence, was used to acquire a series of diffusion-weighted, inversion-recovery data sets at different b values. The resulting two-dimensional (2D) NMR data set can be subjected to a 2D ILT analysis to produce a relaxo-diffusigram. Alternatively, the 2D NMR data set can be analyzed by sequential 1D analyses, using either numerical ILT or sums of discrete exponentials. If the longitudinal relaxation dimension is analyzed first, the water ADC can then be accurately calculated for each compartment from the second 1D analysis. The implementation of the DW-IRSE NMR method is demonstrated using yeast cells suspended in CR-containing medium. This reasonably well-characterized model system is useful for conveying the nuances of the technique and facilitating the quantitative validation of the method.

THEORY

Bloch Equations for DW-IRSE Pulse Sequence

Figure 1 shows a diffusion-weighted, inversion-recovery spin-echo (DW-IRSE) pulse sequence. The dependence of the nuclear

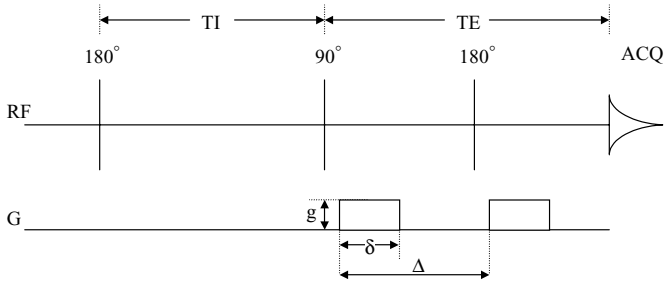

FIG. 1. Diffusion-weighted inversion-recovery spin-echo (DW-IRSE) pulse sequence. T_1-weighting is performed by varying the inversion time (TI) and maintaining a constant echo time (TE). For the isotropic yeast-cell suspension sample, diffusion gradients were applied simultaneously along three orthogonal gradient directions (G_x, G_y, G_z). The diffusion gradient pulse parameters are diffusion gradient separation (Δ), strength (g), and duration (δ).

magnetization on the T_1 and T_2 relaxation times and the diffusion coefficient (D) for the spin-bearing molecule in a homogenous sample excited by the DW-IRSE pulse sequence can be derived from the Bloch equations,

$$M(T_1, T_2, D) = M_0\left(1 - 2\alpha e^{-\frac{\mathrm{TI}}{T_1}}\right)e^{-\frac{\mathrm{TE}}{T_2}}e^{-\gamma^2\delta^2g^2D[\Delta-(\delta/3)]}, \quad [1]$$

where $M(T_1, T_2, D)$ is the magnetization measured at a particular inversion time (TI), echo time (TE), diffusion gradient pulse separation (Δ), diffusion gradient strength (g), and diffusion gradient duration (δ). The equilibrium magnetization is denoted by M_0, α (ranging from 0 to 1) is the efficiency of the inversion pulse, and γ is the gyromagnetic ratio. The quantity $\gamma^2\delta^2g^2[\Delta - (\delta/3)]$ is often referred to as the b value (*18*).

For measurements made at a constant TE, Eq. [1] can be rewritten to express M with the constant T_2 relaxation effects being subsumed with M_0 to give M_0':

$$M(T_1, D) = M_0'\left(1 - 2\alpha e^{-\frac{\mathrm{TI}}{T_1}}\right)e^{-\gamma^2\delta^2g^2D[\Delta-(\delta/3)]}. \quad [2]$$

When the IR data are collected at a given TE and diffusion-weighting, the T_1 relaxation time and equilibrium magnetization can be calculated by fitting with

$$M(T_1) = M_0''\left(1 - 2\alpha e^{-\frac{\mathrm{TI}}{T_1}}\right), \quad [3]$$

where M_0'' contains the effects of both transverse relaxation and diffusion. To measure the molecule's D value, the IR data collection can be repeated at different diffusion g values at constant TE. At each constant g value, the DW-IRSE data set is then fitted with Eq. [3] for M_0'', T_1, and α. The value of D can be calculated from the dependence of M_0'' on $\gamma^2\delta^2g^2[\Delta - (\delta/3)]$.

For a sample containing two components in exchange equilibrium, for example, signals from the IC and EC compartments having different relaxation times and self-diffusion coefficients,

Eq. [1] can be modified to include the signals arising from each component,

$$\begin{aligned} M(T_{1a}, T_{1b}, T_{2a}, T_{2b}, D_a, D_b) &= M_{0a}\left(1 - 2\alpha e^{-\frac{\mathrm{TI}}{T_{1a}}}\right) e^{-\frac{\mathrm{TE}}{T_{2a}}} e^{-\gamma^2\delta^2 g^2 D_a[\Delta-(\delta/3)]} \\ &\quad + M_{0b}\left(1 - 2\alpha e^{-\frac{\mathrm{TI}}{T_{1b}}}\right) e^{-\frac{\mathrm{TE}}{T_{2b}}} e^{-\gamma^2\delta^2 g^2 D_b[\Delta-(\delta/3)]}, \end{aligned} \quad [4]$$

where M_{0a} and M_{0b} are the apparent equilibrium magnetizations of components a and b, respectively, and T_{1a} and T_{1b} are the respective apparent longitudinal relaxation time values. The respective apparent transverse relaxation times are given by T_{2a} and T_{2b}, while D_a and D_b are the respective component apparent diffusion coefficients. The inversion efficiency, α, is assumed to be the same for both components.

As shown in Eq. [2], experiments conducted at a constant TE can be rewritten to express M with constant transverse relaxation effects as

$$\begin{aligned} M(T_{1a}, T_{1b}, D_a, D_b) &= M'_{0a}\left(1 - 2\alpha e^{-\frac{\mathrm{TI}}{T_{1a}}}\right) e^{-\gamma^2\delta^2 g^2 D_a[\Delta-(\delta/3)]} \\ &\quad + M'_{0b}\left(1 - 2\alpha e^{-\frac{\mathrm{TI}}{T_{1b}}}\right) e^{-\gamma^2\delta^2 g^2 D_b[\Delta-(\delta/3)]}. \end{aligned} \quad [5]$$

For DW-IRSE experiments conducted with constant diffusion-weighting as well as TE, the respective T_1 relaxation times and component magnetizations can be determined from a biexponential fitting of the data with

$$M(T_{1a}, T_{1b}) = M''_{0a}\left(1 - 2\alpha e^{-\frac{\mathrm{TI}}{T_{1a}}}\right) + M''_{0b}\left(1 - 2\alpha e^{-\frac{\mathrm{TI}}{T_{1b}}}\right) \quad [6]$$

and solving for M''_{0a}, M''_{0b}, T_{1a}, T_{1b}, and α. Then, as shown previously, the component diffusion coefficients (D_a and D_b) can be calculated from the dependence of M''_{0a} and M''_{0b} on $\gamma^2\delta^2 g^2[\Delta - (\delta/3)]$. The fractions of the signal from component a, f_a, and component b, f_b, can be calculated from the magnetizations at $g = 0$, $M''_{0a}(0)$ and $M''_{0b}(0)$, that is, when no diffusion-weighting is applied:

$$f_a = \frac{M''_{0a}(0)}{M''_{0a}(0) + M''_{0b}(0)} \quad [7a]$$

and

$$f_b = \frac{M''_{0b}(0)}{M''_{0a}(0) + M''_{0b}(0)}. \quad [7b]$$

This two-site approximation assumes that components a and b are the only signal sources in the sample (i.e., $f_a + f_b = 1$).

Relaxographic NMR Timescales

Because T_1, T_2, diffusion, and equilibrium exchange all have important effects in these experiments, we define here the transverse and longitudinal timescales. The transverse relaxographic timescale is given by the expression $|(r_{2o} - r_{2i})[\mathrm{CR_o}] + (R_{2o0} - R_{2i0}) + \gamma^2\delta^2 g^2(D_o - D_i)|^{-1}$, where the r_x are the relaxivities, D represents the apparent diffusion values, and the R_x are the relaxation rate constants $[(T_x)^{-1}]$. The o and i subscripts designate the EC (outside) and IC (inside) spaces, respectively, which, for the R_x and D properties, signify the values in the absence of exchange. This expression reduces to the intrinsic transverse relaxographic timescale ($|R_{2o0} - R_{2i0}|^{-1}$) in the case of $[\mathrm{CR_o}] = 0$ (no CR) and $g = 0$ (diffusion gradient amplitude set to zero). Note that it is the combination of intrinsic relaxation rate constants, the CR concentration, and the difference in the IC and EC diffusion values that set the transverse relaxographic timescale. Therefore, the relevant exchange regime will be determined by comparison of the exchange time with this combination of all three of these quantities. When $g \neq 0$, we refer to the transverse relaxographic timescale as the "diffusigraphic" timescale with the understanding that the effects of the CR addition and the intrinsic transverse relaxation rates are still present. The longitudinal relaxographic timescale is given by $|r_{1o}[\mathrm{CR_o}] + (R_{1o0} - R_{1i})|^{-1}$.

METHODS

Yeast Preparation

Approximately 1.5 g of common dry baking yeast (*Saccharomyces cerevisiae*, Fleishmann's Yeast, Inc., Oakland, CA) was rehydrated at room temperature in a 50-mL centrifuge tube with 35 mL of distilled H_2O. The yeast suspension was bubbled with medical-grade air, and, after a starving period of 3 h, the suspension was centrifuged for 8 minutes at 3500 rpm (IEC-Centra8 Centrifuge, International Equipment Co.). The supernatant was discarded, and the packed yeast cells were resuspended in a solution of 3 mM gadopentate dimeglumine (Gd-DTPA^{2-}, Magnevist, Berlex, Wayne, NJ) and centrifuged. The cells were washed three times with the 3-mM Gd-DTPA^{2-} solution. After the final washing, the packed yeast cell pellet was weighed and the wet/dry mass ratio adjusted to 3.25 : 1.0 with an additional amount of the 3-mM Gd-DTPA^{2-} solution. Preliminary experiments indicated that this ratio value and this [CR] yielded a cell suspension with an IC : EC ^1H_2O apparent magnetization ratio ($f_b : f_a$) near unity and that was viscous enough to remain suspended (i.e., there was no settling) during the experiment. After wet/dry mass ratio adjustment, the cells were resuspended with agitation. Approximately 0.2 mL of the Gd-doped yeast-cell suspension was then transferred to a standard 1.0-mL syringe and placed in a radiofrequency (RF) coil and positioned in the magnet. Experiments were performed on 7 separate yeast-cell preparations. For comparison, an experiment was conducted on one CR-free yeast-cell sample. The preparation of this sample was the same except the yeast cells were washed and

resuspended (wet/dry mass ratio adjusted to 3.25 : 1.0) with distilled H_2O.

NMR Experiments

All data were acquired with a GE CSI-II 2.0T/45-cm imaging spectrometer operating at 85.56 MHz for ^1H and equipped with ±20 G/cm self-shielded gradients. NMR measurements were performed on the entire yeast sample using a 7.25-mm diameter, 8-turn solenoid transceiver RF coil. The magnet-bore temperature was 17°C. NMR data were acquired using the DW-IRSE pulse sequence (Fig. 1). Thirty-two inversion times (TI), with logarithmic temporal spacing ($TI = TI_0 * a^{n-1}$, $TI_0 = 5.0$ ms, $a = 1.257$, $n = 32$) and two signal averages, were used to measure each T_1-relaxation curve. Other acquisition parameters were $\Delta = 46.5$ ms, $\delta = 6.0$ ms, TR = 6.1 s, and TE = 55.0 ms. Diffusion-weighting was accomplished using half-sine-shaped magnetic field gradient pulses simultaneously applied in three orthogonal directions with effective amplitudes (g) of 2.6 to 31.18 G/cm, incremented in steps of 2.6 G/cm (12 diffusion gradient strengths). The use of half-sine-shaped diffusion gradient pulses requires a modification to the equations shown under Theory. In this case, the diffusion-weighting term, the b value (*18*), was modified from $\gamma^2\delta^2 g^2[\Delta - (\delta/3)]$ to $\gamma^2\delta^2(2/\pi)^2 g^2[\Delta - (\delta/4)]$. Half-echoes were acquired with a spectral width of ±5 kHz and 8192 data points.

Data Analysis

Raw DW-IRSE data were transferred to a PC and processed using software written in the C programming language (Borland International, Inc., Scotts Valley, CA). The phase-corrected water resonance in each spectrum was fitted to a Lorentzian function and the peak height was extracted. The resulting data were analyzed by three different methods: (I) An entire 2D data set (TI and g incrementations) from a preparation was submitted for a 2D numerical ILT analysis using the program CONTIN (*8–12, 15, 16, 19*). This produced a 2D contour plot (*19*) with T_1 for one dimension and D for the other. (II) The TI recovery at each g value was subjected to an independent numerical ILT analysis. This yielded a stacked plot of longitudinal relaxograms with g as the vertical dimension (*9*). (III) The IR curve obtained at each diffusion gradient value was separately fitted with both the monoexponential (Eq. [3]) and biexponential (Eq. [6]) models using 3- and 5-parameter (respectively) constrained, nonlinear least-squares Levenberg–Marquardt fitting algorithms written in the Interactive Data Language (IDL, Research Systems, Inc., Boulder, CO) (*9, 13, 14*). Fitting constraints were defined such that no fitted relaxation time parameter could be negative or greater than twice the bulk water relaxation time constant. Data were separately fitted with both the monoexponential and biexponential equations because at high diffusion weighting the signal contribution of the fast-relaxing component becomes negligible and the composition of the IR curve changes from two components to one (*9*).

To determine this transition, both discrete exponential models were tested on every data set. To determine the most appropriate model to describe the IR data at each diffusion-gradient value, F-statistics were calculated. The F-statistic is a measure of model appropriateness based on the ratio of the sum of residual squares of the fitted data of each model weighted by the number of degrees of freedom for the model. In general, if two variables U and V have independent χ^2 with degrees of freedom ν_U and ν_V, respectively, the F-statistic is the distribution of the random variable F, which is defined as

$$F = \frac{U/\nu_U}{V/\nu_V}. \qquad [8]$$

For this application, the F-statistic was used to test the hypothesis that the biexponential model is statistically different than the monoexponential model. Equation [8] was modified to

$$F = \frac{SS_E/\nu_E}{SS_F/\nu_F}, \qquad [9]$$

where SS_F is the sum of squares of the residuals and ν_F is the number of degrees of freedom for the *full* biexponential model in Eq. [6]. SS_E is the sum of squares of the residuals and ν_E is the number of degrees of freedom for the *extra* terms of the biexponential model as compared to the monoexponential model in Eq. [3] ($SS_E = SS_{\text{mono}} - SS_F$). As the IR data sets change from biexponential to monoexponential, the F-statistic (F in Eqs. [8] and [9]) approaches zero, indicating that the monoexponential model is statistically equal to the biexponential model; therefore, the biexponential hypothesis is not true and the monoexponential model is the most appropriate. The output of the fitting program was: (1) M_0'', T_1, and α from a single-component fitting with Eq. [3]; (2) M_{0a}'', M_{0b}'', T_{1a}, T_{1b}, and α from a two-component fitting with Eq. [6]; and (3) the F-statistic.

Finally, the natural logarithms of the fitted M_{0a}'' and M_{0b}'' values were plotted versus the $\gamma^2\delta^2(2/\pi)^2 g^2[\Delta - (\delta/4)]$ values, and D_a and D_b were calculated using a nonweighted, linear least-squares regression fit to the equation,

$$\ln\left(\frac{M_{0i}''}{M_{0i}''(0)}\right) = -\gamma^2\delta^2\,(2/\pi)^2\, g^2[\Delta - (\delta/4)]D_i, \qquad [10]$$

where subscript i denotes a or b. Assuming the two components are the only sources of signal, $M_{0a}''(0)$ and $M_{0b}''(0)$ were used to calculate the normalized fractional contributions when $g = 0$. The fractional contributions of components a and b are denoted f_a and f_b, respectively, and were calculated as the ratio of $M_{0a}''(0)$ or $M_{0b}''(0)$ to the total signal according to Eqs. [7a] and [7b]. For consistency, signal a is equated with the fast relaxation component and signal b with the slow component. We refer to this third method as sequential 1D analyses (longitudinal relaxation analysis *followed* by diffusion decay analysis).

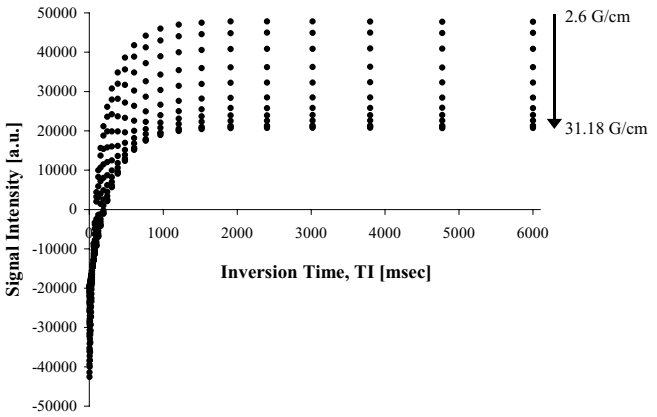

FIG. 2. DW-IRSE data set for a representative yeast-cell suspension in 3 mM Gd-DTPA^{2-} with signal intensity plotted versus inversion time, TI, logarithmically spaced from 5.0 to 6002.9 ms for 12 diffusion gradient strengths ranging from 2.6 to 31.18 G/cm (b values of 3172, 12,688, 28,549, 50,754, 79,303, 114,196, 155,434, 203,016, 256,942, 317,212, 383,827, and 456,786 s/cm^2, respectively). As the diffusion-weighting is increased, the asymptote (M_0) of the measured signal intensity decreases. At high diffusion-weighting, the asymptotes (M_0) of the measured signal intensity curves become closer together as the recovery changes from a two- to one-exponential time function due to quenching of the fast-diffusing component by the strong diffusion gradients.

RESULTS

A set of DW-IRSE curves from a representative preparation (No. 6) is shown in Fig. 2, with signal intensity plotted versus inversion time, TI, for 12 diffusion gradient strengths (g) ranging from 2.6 to 31.18 G/cm (b values of 3172, 12,688, 28,549, 50,754, 79,303, 114,196, 155,434, 203,016, 256,942, 317,212, 383,827, and 456,786 s/cm^2, respectively). Notice that the dynamic range of the IR data decreases with increasing gradient strength. This is because the signal from the faster diffusing component is attenuated by the diffusion gradient to a greater extent than that from the slower diffusing component (*9*). Above some b value, the fast-diffusing component will be completely attenuated before the signal acquisition, and the IR curve will be best described by the single component model. Further, note that the g-induced change in signal intensity at a given TI is not uniform (i.e., the spacing between data points becomes closer at high gradient strengths). This again is due to the differential attenuation of the fast-diffusing component relative to the slow-diffusing component.

Contour plots in Fig. 3 present results from 2D numerical ILT analyses (method I). The vertical, relaxographic dimensions measure the logarithm of T_1 with units of ms. The horizontal, diffusigraphic dimensions measure the logarithm of D with units of cm^2/s. The left plot (Fig. 3a) presents the results from the preparation with [CR] = 0 mM. This plot shows two peaks whose $T_1 : D$ coordinates are 496 ms : 0.033×10^{-5} cm^2/s (25%) and 496 ms : 1.22×10^{-5} cm^2/s (75%), respectively. (The coordinates given are those of the peak maxima, and the percentage contributions represent the relative peak volumes. The four contour levels seen in the left plot have relative values: 1 : 1.6 : 6 : 12.) The right plot (Fig. 3b) presents the results from a preparation (No. 6) with [CR] = 3 mM. It shows two peaks whose $T_1 : D$ coordinates are 272 ms : 0.033×10^{-5} cm^2/s (48%) and 61 ms : 1.22×10^{-5} cm^2/s (52%), respectively. (The contour levels have relative values: 1 : 2 : 3.2 : 4.8.)

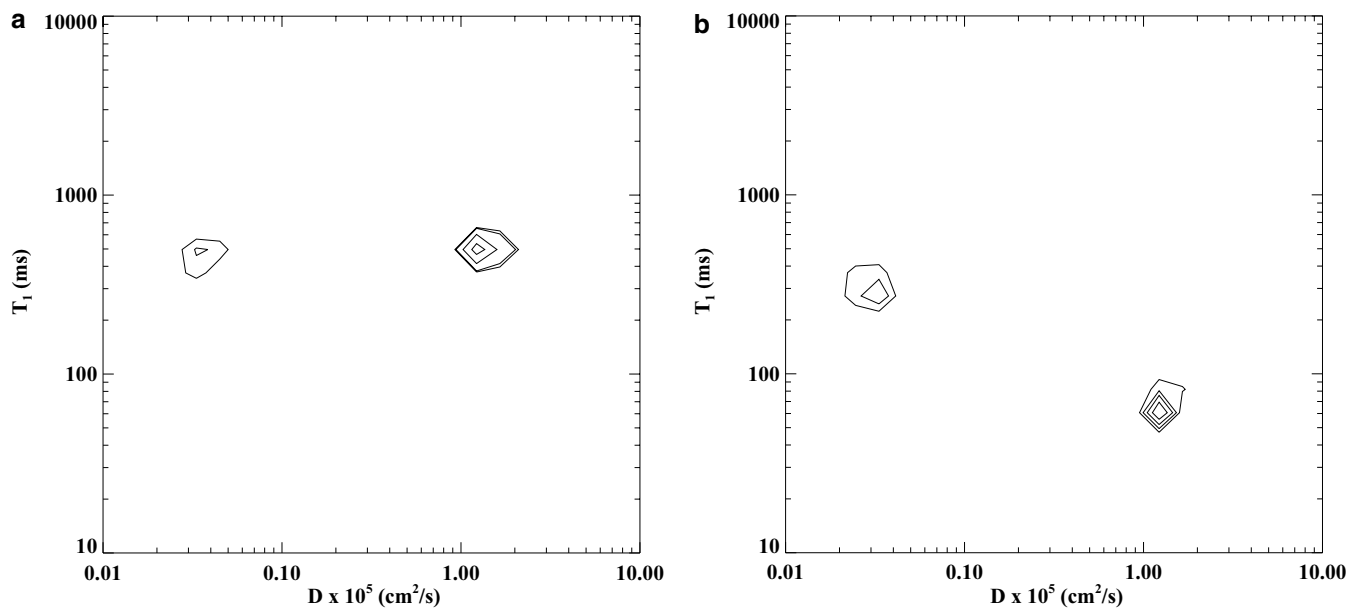

FIG. 3. Contour plots of the relaxo-diffusigrams resulting from 2D numerical ILT analyses of data sets of the type seen in Fig. 2: (a) from a preparation with extracellular [GdDTPA^{2-}] = 0 mM; (b) from a preparation with extracellular [GdDTPA^{2-}] = 3 mM. The ordinates measure the logarithm of T_1, in ms. The abscissae measure the logarithm of D, in cm^2/s. The four contour levels have the relative arbitrary values of 1 : 1.6 : 6 : 12 in (a) and 1 : 2 : 3.2 : 4.8 in (b).

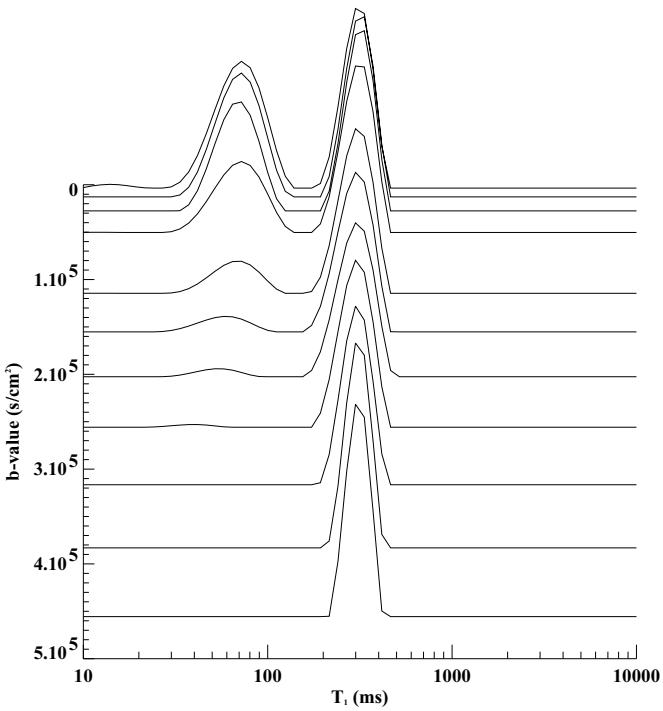

FIG. 4. A stacked plot of selected longitudinal relaxograms obtained at different b values. These result from the 1D numerical ILT of the inversion recovery data for the data in Fig. 2. The abscissa measures the logarithm of T_1, in ms. The b values range from 3172 s/cm^2 (top) to 456,786 s/cm^2 (bottom). The incrementation is given in the text.

Figure 4 presents a stacked plot of the longitudinal relaxograms (the abscissa measures the logarithm of T_1, in ms) for different b values (obtained from data analysis method II), for the same 3-mM CR preparation (No. 6) of Figs. 2 and 3b. The series of T_1 relaxograms was obtained from the 1D ILT of the corresponding IR curves shown in Fig. 2. The b values range from 3172 s/cm^2 at the top to 456,786 s/cm^2 at the bottom, with the incrementation listed above. The average positions (and areas) of the EC and IC peaks are 64 ms (54% at b value $= 0$) and 307 ms (46% at b value $= 0$), respectively. A *subsequent* numerical ILT diffusigraphic analysis, conducted on the areas of the Fig. 4 EC and IC peaks, yielded D values of 1.29×10^{-5} cm^2/s and 0.032×10^{-5} cm^2/s, respectively.

The results for the final data analysis method (III) were obtained from the same data set shown in Figs. 2–4 (preparation No. 6) and illustrate the sequential 1D analyses using discrete exponential fittings. Figure 5 shows a comparison of the bi- and monoexponential fittings for the data acquisitions with the 2.6 G/cm (minimum) and 31.18 G/cm (maximum) diffusion-gradient pulses. The natural logarithm of the magnetization function is shown for easier visualization of the data nature. The IR data acquired at a diffusion-weighting of 2.6 G/cm (●) are fitted with both the biexponential (—) and monoexponential (---) models. The biexponential fitting is clearly more appropriate for these data and this is statistically supported with an F-statistic $\gg 0$. Also in Fig. 5, the IR data acquired at the much larger diffusion-weighting of 31.18 G/cm (×) are fitted with both the biexponential (—) and monoexponential models. For this data set, the monoexponential fitting (---) is not visible because it is coincident with the biexponential fitting. In this case, the monoexponential model is more appropriate (F-statistic ~ 0).

Each IR curve in the Fig. 2 data set was fitted with the biexponential model to determine M''_{0a}, M''_{0b}, T_{1a}, T_{1b}, and α, and also with the monoexponential model to determine M''_0, T_1, and α. The fitting of each of the 12 IR curves was performed independently (fitting constraints and initial parameters were the same for each iteration). For this representative preparation, the average calculated fast-relaxing T_1 value (T_{1a}) was 65 ± 2 ms and the average slow-relaxing T_1 value (T_{1b}) was 304 ± 5 ms.

From the model fittings, M''_0, M''_{0a}, and M''_{0b} were extracted at each g value and plotted versus the b value. Figure 6 shows M''_0, M''_{0a}, and M''_{0b} (arbitrary units) derived from the data of the representative preparation used for Figs. 2–5. The triangles (▲) and the open circles (○) are the calculated magnetization values for the fast-relaxing (M''_{0a}) and the slow-relaxing (M''_{0b}) components, respectively, from the biexponential model. The closed circles (●) are the fitted M''_0 values from the monoexponential model. Note that as the b value is increased, the contribution of the fast-relaxing component (M''_{0a}) vanishes, and the fitted M''_0 values asymptotically approach M''_{0b}. Fitting errors were apparent in the biexponential model for b values greater than 300,000 s/cm^2 (for obvious reasons) and these points have been omitted from Fig. 6.

The natural logarithm or the ▲ and ○ curves in Fig. 6 were each fitted using Eq. [10] to calculate the fractional contributions

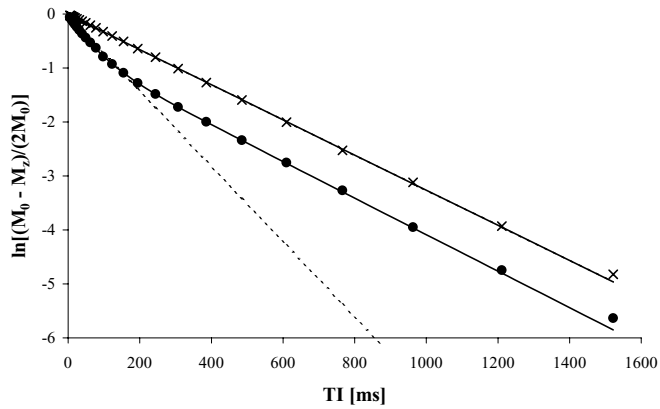

FIG. 5. Biexponential (—) and monoexponential (---) model fittings to IR data sets obtained with diffusion-weighted gradient amplitudes of 2.6 G/cm (●) and 31.18 G/cm (×) for the yeast-cell sample of Fig. 2. The natural logarithm of the relaxation functions (*20*) is shown to aid in visualizing the data characters. The 2.6-G/cm data set (●) is best described by the biexponential model; note the monoexponential fit (dashed line) markedly deviates from the experimental points. The monoexponential model and the biexponential model match the IR data for the set acquired at a diffusion-weighting of 31.18 G/cm (×), which indicates that the biexponential model "over fits" this data set and the monoexponential model is most appropriate.

TABLE 1

Apparent Compartmental Relaxation Times (T_{1a} and T_{1b}) with Standard Deviations (σ), Diffusion Coefficients (D_a and D_b), and Fractional Contributions (f_a and f_b) without Diffusion Attenuation (i.e., $g = 0$) from Experiments on Seven Separate Yeast-Cell Suspensions Determined with Sequential 1D Exponential Analyses

Preparation	T_{1a} (σ) [ms]	T_{1b} (σ) [ms]	D_a [$\times 10^{-5}$ cm^2/s]	D_b [$\times 10^{-5}$ cm^2/s]	f_a ($g = 0$) [unitless]	f_b ($g = 0$) [unitless]
1	65 (2)[a]	291 (4)[a]	1.22[d]	0.026[e]	0.54	0.46
2	67 (1)	301 (3)	1.26	0.026	0.53	0.47
3	67 (2)	289 (3)	1.11	0.024	0.54	0.46
4	65 (3)	292 (2)	1.22	0.021	0.54	0.46
5	64 (2)	294 (3)	1.20	0.020	0.59	0.41
6	65 (2)	304 (5)	1.24	0.023	0.53	0.47
7	65 (2)	294 (4)	1.10	0.021	0.51	0.49
Overall	65 (2)[b]	295 (6)[b]	1.19 (0.06)[c]	0.023 (0.002)[c]	0.54 (0.02)[c]	0.46 (0.02)[c]

[a] The intraexperiment σ is from the T_{1a} and T_{1b} values obtained from the 9 (out of a total of 12) DW-IR data sets fitted to the biexponential model (Eq. [6]).
[b] σ is calculated from the means and σ of the experiments on the 7 preparations.
[c] σ is calculated from the means of the experiments on the 7 preparations.
[d] Linear regression $R^2 > 0.80$ for fit of M''_{0a} versus the b value.
[e] Linear regression $R^2 > 0.98$ for fit of M''_{0b} versus the b value.

(at $g = 0$) and the component diffusion coefficients. For these data, the fractional contribution of the fast-relaxing component (▲), f_a, was 0.53, and the fractional contribution of the slow-relaxing component (○), f_b, was 0.47. The diffusion coefficient of the fast-relaxing component, D_a, was 1.24×10^{-5} cm^2/s, and the diffusion coefficient of the slow-relaxing component, D_b, was 0.023×10^{-5} cm^2/s. The R^2 linear regression coefficients (Eq. [10]) for D_a and D_b were 0.80 and 0.99, respectively. Table 1 contains the results from sequential 1D exponential analyses of the experiments on all seven different yeast-cell preparations. The T_1 values are presented as the means and standard deviations (σ), which were calculated within each preparation, and over all preparations.

Finally, given the significant difference in D_a and D_b in the yeast-cell preparation and the consequent slow-exchange diffusigraphic conditions, a direct 1D diffusigraphic analysis of the b-space decay was conducted to further validate the diffusion coefficient values obtained using analysis methods I–III. If a 1D diffusigraphic analysis of the b-space decay data from a CR-free sample is conducted, two diffusigraphic peaks are obtained (*15*). For the data in Fig. 2, magnetization values at the longest TI value (i.e., under fully relaxed conditions and thus without any T_1 weighting) were fitted versus the b value using the discrete biexponential approach. The resulting diffusion coefficients were $D_a = 1.17 \pm 0.003 \times 10^{-5}$ cm^2/s ($56 \pm 3\%$) and $D_b = 0.017 \pm 0.004 \times 10^{-5}$ cm^2/s ($44 \pm 3\%$), which are also in good agreement with the mean values in Table 1.

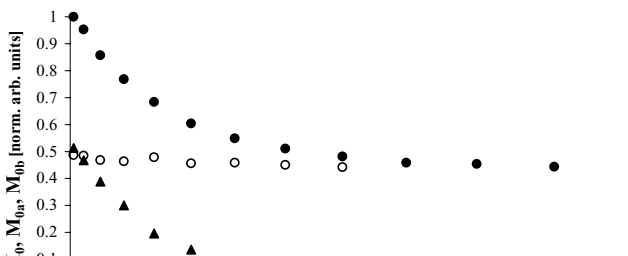

FIG. 6. The normalized calculated M''_{0a}, M''_{0b}, and M''_0 values for the representative data set shown in Fig. 2. The triangles (▲) and the open circles (○) are the fast-relaxing M''_{0a} and slow-relaxing M''_{0b} components, respectively, calculated using the biexponential model. The solid circles (●) are the M''_0 values calculated using the monoexponential model. Note that M''_0 approaches the slow-relaxing, slow-diffusing component (IC) described by M''_{0b}.

DISCUSSION AND CONCLUSIONS

This paper presents an NMR method for measuring compartment-specific water diffusion coefficients. The method is based on relaxography (*8*), employing an EC CR to distinguish the IC and EC water signals based on differences in their respective T_1 relaxation times. By incorporating diffusion encoding into the relaxography experiment, compartment-specific ADC values can be measured from compartmental signals that have been separated and identified in the relaxographic domain. The NMR method has been implemented using a DW-IRSE pulse sequence (Fig. 1), which was used to acquire a series of diffusion-weighted, IR data sets (at different b values) from yeast cells suspended in 3 mM Gd-DTPA^{2-} (Fig. 2). The wet/dry mass ratio of the yeast (3.25 : 1.0) and the CR concentration were intentionally optimized to clearly demonstrate the performance of the NMR method as well as facilitate the quantitative validation of the technique.

The large differences in diffusion coefficients between the IC and EC space of yeast-cell suspensions do make it possible to measure the compartment-specific diffusion coefficients

directly, without the need for CR (*15, 17*) or use of the DW-IRSE method. However, for the work reported here, these features were used to advantage to further validate the values of the compartment-specific diffusion coefficients derived from the DW-IRSE method. Furthermore, for *in vivo* applications in tissue, accurate compartment-specific diffusion coefficients (as well as compartment sizes) have yet to be convincingly measured by direct biexponential fitting of the diffusion-attenuation curves. In these cases, the DW-IRSE approach should yield accurate compartment-specific ADC values, even when the respective compartmental ADC values may be quite similar and difficult to assign unambiguously.

In the absence of CR, the intrinsic IC and EC ^1H_2O T_1 values by themselves are not sufficiently different to allow discrimination of these compartments (Fig. 3a), especially when the timescale they represent is compared with the time for the equilibrium transcytolemmal exchange of water (*8*). However, by the natural restriction of CR to the EC space, the T_1 relaxation time of the EC compartment ^1H_2O can be decreased such that the relaxation time constants of the IC and EC space ^1H_2O signals differ by more than a factor of three (Fig. 3b). Simulations have shown that this is the minimum difference necessary to deconvolve correctly a sum of exponentials with a signal-to-noise ratio (SNR) ~50 by fitting with a biexponential model (*13, 14*). The addition of 3-mM CR to the yeast-cell suspension resulted in approximately a factor of five difference (an EC T_1 of 0.061 s vs an IC T_1 of 0.272 s) in the apparent ^1H_2O T_1 relaxation times of the signals from the two compartments (see also data in Table 1). Note that both peaks in Fig. 3b are shifted to smaller T_1 values by the CR, although it is quite clear that the peak with the larger D value is significantly more displaced. This is expected since the CR acts as a shift reagent in relaxographic space and the transcytolemmal water exchange is facile (*8*). By contrast, the compartmental diffusion coefficients remain essentially unchanged upon addition of the CR. This result is very encouraging and is consistent with diffusion coefficient measurements made on homogeneous water phantoms doped with different CR concentrations, where the presence of CR by itself does not alter the diffusion coefficient of water molecules (unpublished results).

The contour plots shown in Fig. 3 are also useful for visualizing the qualitative differences between the two samples as a function of CR concentration. Since Gd-DTPA^{2-} is known to be restricted to the extracellular space in this model system (*8*), it is obvious that the most shifted peak should be assigned to the EC signal. This confirms one's intuition with regard to the relative magnitudes of the compartmental water D values in cell suspensions. However, since tissue generally has a higher cell density than is achievable in cell suspensions *in vitro*, the compartmental assignments may not be as obvious in that case, and plots such as those in Fig. 3 could prove to be an important tool for the unambiguous analysis of tissue data.

As shown in Fig. 3 (and Table 1), the IC water apparent D is much smaller than the EC water apparent D due to the diffusion restrictions imposed by the small size of the yeast cells, which we estimated using a standard light microscope to be ~7 μm in outer diameter. For a spherical shape, the intracellular diameter (d_{IC}) of the yeast cell can be estimated from the apparent diffusion coefficient and the diffusion time, as shown by Tanner (*17*):

$$d_{IC} = \sqrt{20 D t_{diff}}. \quad [11]$$

Using values for t_{diff} of 45 ms and $D_{IC} = 0.023 \times 10^{-5}$ cm^2/s (mean value from Table 1) for these experiments, Eq. [11] yields a d_{IC} value of 4.6 μm, which is in good agreement with the value of 4.0 μm reported by Tanner (*17*). The presence of the impermeable cell membrane and small cell size explains why the D_{IC} is so small. By contrast, water diffusing in the EC environment of cell suspensions should have a D value closer to that of free water. At 17°C (the temperature for our yeast-cell diffusion measurements), the diffusion coefficient of bulk water is approximately 1.8×10^{-5} cm^2/s. The reduction in the EC water D relative to the bulk value is presumably caused by restrictions in this concentrated cellular suspension due to the close proximity of the external surfaces of cell membranes. Also, in this particular case, EC water includes water in the periplasmic spaces, which are quite confined (*20*). Still, the diffusion coefficients here differ by a factor of 40, a situation not likely to be encountered in tissue.

The stacked plot of the longitudinal relaxograms as a function of the b value (Fig. 4) is particularly useful for visualizing the relative differences in diffusion attenuation between the two components. With increased diffusion weighting, the fast-relaxing (which is also the fast-diffusing) component is increasingly attenuated and ultimately quenched at higher diffusion-gradient strengths. It has been thoroughly demonstrated that in the presence of CR the peak at smaller T_1 represents the EC signal (*8*). Thus, Fig. 4 shows very clearly that it is the EC signal that is attenuated with increasing b value, as we reported earlier with a preliminary version of Fig. 4 (*9*). By contrast, the intracellular signal exhibits relatively little attenuation (~10%) over this range of b values, due to the severe restriction effects imposed by the small intracellular diameter of the yeast cells. It is important to note that the positions of the T_1 distributions in Fig. 4 are consistent with those in the relaxographic dimension of Fig. 3 (as expected since the ILT analysis was used in both cases). Furthermore, the subsequent 1D ILT diffusigraphic analysis of the areas of the EC and IC T_1 distributions in Fig. 4 yielded compartment-specific diffusion coefficients that were also comparable to those derived from the diffusigraphic dimension of Fig. 3.

Figure 5 shows the results for the final data analysis method (III) applied to the same data set analyzed by ILT methods I and II in Figs. 3 and 4, respectively. It should be noted that results obtained from the discrete exponential fitting of the data obtained at the minimum and maximum b values in Fig. 2 are consistent with the comparable ILT results in Fig. 4. For example, for the 2.6-G/cm (minimum b value) data set in Fig. 5,

the IR data are best fitted with a discrete biexponential. The two T_1 values derived from this analysis are in good agreement with the means of the two T_1 distributions obtained by the 1D ILT analysis of the corresponding data set in Fig. 4. By contrast, for the 31.18-G/cm (maximum b value) data set in Fig. 5, the longitudinal relaxation data are best fitted using a monoexponential model. This is consistent with the corresponding maximum-b-value data set in Fig. 4, where the fast-diffusing, fast-relaxing T_1 component is completely quenched at this diffusion-sensitive gradient strength, leaving only the signal from the slow-diffusing, slow-relaxing T_1 component.

Figure 6 shows the results from the discrete exponential analysis of each IR curve in Fig. 2, which yields diffusion-weighted M''_{0a} and M''_{0b} values (for each T_1 component, T_{1a} and T_{1b}) as a function of the b value. The longitudinal relaxation data were fitted with both bi- and monoexponential functions to determine which model best described the data. At b values of insufficient magnitude to completely quench the fast-diffusing, fast-relaxing T_1 component, the biexponential model provided the best fit to the data. At higher b values, the fast-diffusing, fast-relaxing T_1 component was completely quenched (again, as seen in Fig. 4 as well as the maximum b value data in Fig. 5), and the monoexponential function was the most appropriate fitting model for estimating M''_0. As seen in Fig. 4, with increasing diffusion-weighting, the fast-diffusing, fast-relaxing T_1 component in Fig. 6 is increasingly attenuated by the strong gradient and is ultimately quenched at b values above 300,000 s/cm^2. It is important to note that the average T_{1b} (the slow-relaxing, slow-diffusing component of the two-component signal) obtained from the biexponential analysis is 304 ± 5 ms, which statistically matches the T_1 value derived from the monoexponential fitting model at high b values (306 ± 1 ms). Since the system is well described with one component at high diffusion-gradient strengths, the fact that these T_1 values are the same gives confidence that the same water population is being measured for both cases.

Notice that in Fig. 6, the change in M''_{0a} and M''_{0b} values as a function of the b value exactly parallels the change in the corresponding areas under the EC and IC T_1 distributions shown in Fig. 4. As was the case for the data in Fig. 4, the signal from the IC water (M''_{0b}) was not significantly attenuated ($\sim$10%) over this range of b values due to significantly restricted water diffusion in the IC space. The compartment-specific diffusion coefficients calculated from the slopes of the natural logarithm of the diffusion attenuation curves in Fig. 6 (and summarized in Table 1 for all seven yeast-cell preparations) are in good agreement with the results from the diffusigraphic analysis of the data in Fig. 4 (method II) as well as those in the Fig. 3 2D plot (method I). Furthermore, the compartment-specific diffusion coefficients obtained by all three analysis methods are in good agreement with the results obtained by direct 1D diffusigraphic analysis of the b-space data (diffusigraphy (*15*)) in the absence of T_1 weighting. This result provided further confidence in the validity of the results obtained using the DW-IRSE NMR method as well as data analysis methods I–III.

Methods I and II (used to analyze the data in Figs. 3 and 4, respectively) employ numerical, continuous relaxography (*8*) to assay T_1 relaxation time differences in the compartmental signal contributions. That is, numerical ILT analysis (*10–12*) is used to calculate the continuous relaxation time distributions from a sample. A disadvantage of this approach is that the ILT method requires a measured value of M_0 for the sample, which results in long experiment times. Fitting the IR data with the 5-parameter biexponential model (method III) does not require an M_0 estimate since it is a fitted parameter, thus allowing smaller TI and TR values to be used, resulting in reduced experiment times. Consequently, implementation of the NMR method with subsequent analysis using method III was deemed to be the most time-efficient experimental approach to these studies.

Another aspect of the numerical ILT method is that the width of the relaxographic peak representing a given compartment can be significantly affected by user-supplied input parameters to the fitting procedure and inappropriate choices may interfere with the separation of peaks from different compartments. The biexponential fitting relaxographic method avoids this limitation as it fits for the means of the relaxation time distributions determined by the ILT method (*9*). Furthermore, the sequential 1D exponential fitting approach (method III) may be a more quantitatively useful data analysis method since it avoids uncertainties associated with estimating the areas and positions of the distributions derived from the numerical ILT analysis. Finally, method III is more computationally efficient than ILT and results in significantly reduced calculation times, particularly when compared to the 2D ILT data analysis method.

We have explored the limitations of the biexponential fitting method through data simulation. For a two-compartment system, the optimal data conditions call for signal contributions (M_{0a} and M_{0b}) in a ratio of 1 : 1, a T_1 relaxation time difference of at least three ($T_{1b} > 3T_{1a}$), and a SNR greater than 20 (*13*). The data presented in this paper exceed these criteria: The fractional signal contribution ($M_{0a} : M_{0b}$) was 0.54 : 0 : 46 or 1.2 : 1.0; T_{1b} was 4.5 times T_{1a}; and the SNR for a 0.2-mL sample exceeded 500. Extension of this method to an *in vivo* biological system would require careful optimization to establish the appropriate CR concentrations and SNR conditions.

Studies by Labadie *et al.* (*8*) and Stanisz *et al.* (*24*) have shown the efficacy of using MR CRs to discriminate the IC and EC water signals in a biological sample by virtue of their relaxation time differences. These studies demonstrated that the addition of the CR alters the relaxation time constants (T_1 and T_2) of both the EC and IC water signals even though, because of the molecular size, hydrophilicity, and electrical charge of the Gd-DTPA^{2-} anion, the CR remains in the EC space. Equilibrium exchange of water molecules between the IC and the EC environments complicates the measurement of the absolute (i.e., exchangeless) compartmental T_1-relaxation times because mixing of the compartmental water increases the number of molecules that contact the CR. However, it has been shown that the addition of

a sufficient concentration of CR can move the system from the fast-exchange regime (FXR) toward the slow-exchange regime (SXR) (*8, 20, 27*) by reducing the relaxation time of the signal from the EC space water, thereby reducing this exchange effect. One reason for selecting the yeast-cell strain used in these experiments is that the transmembrane exchange is relatively slow as compared to other biological systems, such as red blood cell suspensions (*5*), and even other yeast strains (*8, 17, 20*). In this study, confidence that the yeast-cell suspension was in the SXR on the longitudinal relaxographic timescale was supported by the F-statistic analysis method, which determined that the bi-exponential IR model most appropriately described the data for small diffusion gradient values.

In earlier work, it was found that a yeast sample, prepared as in this paper, with a wet/dry mass ratio (w/d) of 3.47 made a cell suspension in which the fraction of water that was intracellular was 0.36 (*8*). Thus, it is a reasonable linear extrapolation to assume that the smaller w/d value use here (3.25) yields a slightly larger intracellular water fraction of 0.38. Thus, the ratio of IC : EC water here is 0.38 : 0.62, a value approaching 2 : 3.

However, there are a number of factors that affect the relative magnitudes of the compartmental ^1H_2O signals ($M_{0a} : M_{0b}$) actually measured in any given NMR experiment. First, there can be a differential relaxation effect: for example, there is a nonnegligible amount of T_2-weighting in our acquisitions (TE = 55 ms). Since each compartment has a different T_2 value, the signal-intensity ratio for the two compartments will vary depending upon the relative difference in T_2 values for a given experimental echo time. Even in the CR-free sample, the overall ^1H_2O T_2 is 0.290 s; and, therefore, the amount of T_2 attenuation at a TE value of 0.055 s would not be insignificant. In this case, is reasonable to assume that the intrinsic T_2 of the IC signal is somewhat smaller than that of the EC signal for the CR-free sample. Upon addition of the CR, however, the EC T_2 is likely to become significantly reduced with relatively less consequence for the IC T_2 value. To the extent that they differ, this would lead to a decrease in the relative contribution from the EC compartment for a given TE value. Second, there can be an effect due to the fact that the water is in equilibrium exchange between the IC and EC compartments. In earlier work, it was found that the mean intracellular lifetime of a water molecule, τ_b, was 0.67 s for the same strain of yeast studied at ambient temperature (*8, 17*). It is reasonable to assume that it is similar here. Since 0.62 of the water is extracellular, the mean extracellular lifetime, τ_a, is 1.1 s: the exchange is in equilibrium. The exchange rate constant is thus $[(\tau_b)^{-1} + (\tau_a)^{-1}] = 2.4\ s^{-1}$, and the exchange time is the reciprocal of this, 0.42 s. If the exchange time was not sufficiently large on the diffusigraphic timescale (the slow-exchange limit (SXL)), the relative contribution of the component exhibiting the larger D value (EC here) would be diminished and the measured smaller D elevated above its true value (*1*).

In the absence of CR, we observe an IC : EC signal ratio of only ∼1 : 3 (Fig. 3a). This suggests that the T_2 effect is dominant, and that the system is probably near the SXL on the diffusigraphic timescale employed here. For a τ_b of 0.67 s, this is reasonable (*1*). It is important to note, however, that the CR-free system is simultaneously in the *fast*-exchange limit (FXL) on the longitudinal relaxographic timescale (*8*). This is evidenced here by the fact that the T_1 values of the two peaks in Fig. 3a are identical, and the magnitude (0.50 s) is surely too small for the EC ^1H_2O signal in the absence of exchange. Thus, while the CR-free system is surely also in the FXL on the intrinsic transverse timescale, its rendering into the SXL on the diffusigraphic timescale enables differential transverse relaxation to dominate the relative contributions.

When CR is added, the $M_{0a} : M_{0b}$ ratio rises to ∼1 : 1, as found by all three methods (Fig. 3b, Fig. 4, Table 1). (Indeed, the samples were deliberately "titrated" to this condition.) This is probably dominated by a reversal of the T_2 effect. Though the addition of the paramagnetic CR to the EC space decreases the T_2 values of both the EC and IC signals because of the transcytolemmal susceptibility gradient created, this is greater for the EC signal (these cells are roughly spherical) and there is an additional hyperfine catalysis of the EC signal transverse relaxation. Thus, while the overall T_2 value is reduced to 0.058 s (quite near the TE value) by 3-mM extracellular CR, we can assume that much of this comes disproportionately from the EC signal, and its relative contribution is thereby reduced. At the same time, though the exchange kinetics are unaltered by the CR, the system is now rendered into SXR on the longitudinal relaxographic timescale (*8, 20*): two peaks appear in the T_1 projection of Fig. 3b. The peak with the larger T_1 is also shifted because of the transcytolemmal water exchange. A [CR] of 3 mM is not sufficient to move the system to the SXL, however, and in the SXR, the relative contribution of the EC signal is diminished (*8, 20*).

Other NMR methods have attempted to separate the IC and EC water diffusion coefficients in *in vitro* and *in vivo* biological samples. Early experiments by Andrasko (*1*) and Tanner (*17*) suggested that the nonmonoexponential behavior of the diffusion attenuation curve in human red blood cell and yeast-cell preparations respectively resulted from two water populations with different diffusion coefficients. However, nonmonoexponential attenuation may arise from restricted diffusion within a continuous compartment, distinct compartments with different diffusion coefficients, or some combination of both (*21*); and in all cases, water exchange between compartments can further complicate interpretation of the diffusion measurement (*1*). Previous work analyzing rat brain ^1H_2O signals attempted to fit diffusion attenuation curves to biexponential models that represent the water diffusion coefficients in IC and EC spaces (*16, 22*). However, when the diffusion coefficients of the two spaces were considered in the absence of exchange and restrictions, the fitted volume fractions did not agree with the known compartmental fractions (*22, 23*). Because nonmonoexponential attenuation curves have been found in single compartment systems with barriers to diffusion (*21*), the presence of restricting barriers in tissue must also be considered in any successful model.

In this case, the use of a CR to confirm assignments of diffusigraphic peaks could prove invaluable. However, its effects on differential relaxation must be carefully considered, as above.

Recent work has demonstrated some success with analytical models of water dynamics in red blood cell suspensions and in simulations that include ^1H_2O relaxation, tortuosity, restricted diffusion, compartmental exchange (membrane permeability), and cell geometry (*24, 26*). These and other studies have used combined T_2-relaxation and diffusion methods to describe biological tissue using the two-compartment (IC and EC) model (*22–24*). However, as we have seen, T_2 is sensitive to hyperfine, bulk magnetic susceptibility and exchange effects. If not properly accounted, these can contribute to misevaluation of the actual compartmental volume fractions (*22*).

Using CR in a well-understood yeast-cell suspension, we have successfully demonstrated an NMR method for clearly assigning and measuring compartmental apparent diffusion coefficients based on differences in the respective T_1 relaxation times of two compartmental ^1H_2O signals. The application of this method to an animal model could be used to study the *in vivo* compartmental (IC and EC) relaxation time constants and ADCs of tissue such as muscle or brain. Further, tissue changes resulting from injury or disease could be measured with respect to each compartment individually. Specifically, since Moseley *et al.* (*4*) demonstrated a decline in the ADC of cerebral tissue water after cerebral ischemia resulting from stroke, there has much speculation regarding the mechanisms causing the ADC decline. Since it is possible to alter the relaxation time constants of the cerebral EC compartment using intracerebroventricular injection of CR (*27*), it is possible to employ this approach to assign the observed ADC components, determine the cerebral IC and EC apparent ^1H_2O T_1 relaxation times, and the water ADC values (*28*). This could lead to better understanding of the underlying mechanism responsible for the water ADC changes during cerebral ischemia.

ACKNOWLEDGMENTS

We thank Gabor Vétek and Ildiko Palyka for help with initial experiments and Christian Labadie for help with the 2D ILT. We thank the NIH (RO1 GM32125 and RO1 NS40801) and the DOE (Contract AC02-98CH10884) for partial support of this work. Part of this work was performed during the tenure of an Established Investigatorship from the American Heart Association (CHS).

REFERENCES

1. J. Andrasko, Water diffusion permeability of human erythrocytes studied by a pulsed gradient NMR technique, *Biochim. Biophys. Acta* **428,** 304–311 (1976).
2. G. E. Wesbey, M. E. Moseley, and R. H. Ehman, Translational molecular self-diffusion in magnetic resonance image. II. Measurement of the self-diffusion coefficient, *Invest. Radiol.* **19**(6), 491–498 (1984).
3. D. Le Bihan, E. Breton, D. Lallemand, P. Grenier, E. Cabanis, and M. Laval-Jeantet, MR imaging of intravoxel incoherent motions: Application to diffusion and perfusion in neurologic disorders, *Radiology* **161,** 401–407 (1986).
4. M. E. Moseley, Y. Cohen, J. Mintorovitch, J. Kucharczyk, L. Chileuitt, H. Shimizu, F. Wendland, and P. R. Weintein, Early detection of regional cerebral ischemia in cats: Comparison of diffusion- and T_2-weighted MRI and spectroscopy, *Magn. Reson. Med.* **14,** 330–346 (1990).
5. L. L. Latour, K. Svoboda, P. P. Mitra, and C. H. Sotak, Time-dependent diffusion of water in a biological model system, *Proc. Natl. Acad. Sci. U.S.A.* **91,** 1229–1233 (1994).
6. P. van Gelderen, M. H. M. de Vleeschouwer, D. DesPres, J. Pekar, P. C. M. van Zijl, and C. T. W. Moonen, Water diffusion and acute stroke, *Magn. Reson. Med.* **31,** 154–163 (1994).
7. T. Q. Duong, J. J. H. Ackerman, H. S. Ying, and J. J. Neil, Evaluation of extra- and intracellular apparent diffusion in normal and globally ischemic rat brain via ^{19}F NMR, *Magn. Reson. Med.* **40,** 1–13 (1998).
8. C. Labadie, J.-H. Lee, G. Vétek, and C. S. Springer, Jr., Relaxographic imaging, *J. Magn. Reson. B* **105,** 99–112 (1994).
9. S. S. Han, G. Vétek, M. D. Silva, C. S. Springer, Jr., and C. H. Sotak, Apparent diffusion coefficients of intra- and extracellular water in yeast suspensions measured by combined diffusion and relaxography, *Proc. Int. Soc. Magn. Reson. Med.* **6,** 535 (1998).
10. S. W. Provencher, A constrained regularization method for inverting data represented by linear algebraic or integral equations, *Comput. Phys. Commun.* **27,** 213–227 (1982).
11. S. W. Provencher, CONTIN: A general purpose constrained regularization program for inverting noisy linear algebraic and integral equations, *Comput. Phys. Commun.* **27,** 229–242 (1982).
12. S. W. Provencher and V. G. Dovi, Direct analysis of continuous relaxation spectra, *J. Biochem. Biophys. Methods.* **1,** 313–318 (1979).
13. M. D. Silva, S. S. Han, and C. H. Sotak, Effects of signal-to-noise and parametric limitations on fitting biexponential magnetic resonance (MR) inversion-recovery curves using a constrained nonlinear least squares algorithm, *in* "Proc., IEEE 24th Annual Northeast Bioeng. Conf., 1998," p. 35.
14. R. M. Kroeker and R. M. Henkelman, Analysis of biological NMR relaxation data with continuous distributions of relaxation times, *J. Magn. Reson.* **69,** 218–235 (1986).
15. G. Vetek, I. Palyka, C. H. Sotak, and C. S. Springer, CR-free discrimination of intra- and extracellular ^1H_2O signals from yeast cell suspensions by diffusion-space relaxography (diffusigraphy), *Proc. Soc. Magn. Reson.* **2,** 1051 (1994).
16. J. Pfeuffer, S. W. Provencher, and R. Gruetter, Water diffusion in rat brain in vivo as detected at very large b values is multicompartmental, *Magn. Reson. Mater. Phys. Biol. Med.* **8,** 98–108 (1999).
17. J. E. Tanner, Intracellular diffusion of water, *Arch. Biochem. Biophys.* **224,** 416–428 (1983).
18. D. Le Bihan, Molecular diffusion nuclear magnetic resonance imaging, *Magn. Reson. Q.* **7,** 1–30 (1991).
19. J.-H. Lee, C. Labadie, C. S. Springer, and G. S. Harbison, Two-dimensional inverse Laplace transform NMR: Altered relaxation times allow detection of exchange correlation, *J. Am. Chem. Soc.* **115,** 7761–7764 (1993).
20. C. S. Landis, X. Li, F. W. Telang, P. E. Molina, I. Palyka, G. Vetek, and C. S. Springer, Equilibrium transcytolemmal water-exchange kinetics in skeletal muscle *in vivo*, *Magn. Reson. Med.* **42,** 467–478 (1999).
21. K. G. Helmer, B. J. Dardzinski, and C. H. Sotak, The application of porous media theory to the investigation of time-dependent diffusion in i*n vivo* systems, *NMR Biomed.* **8,** 297–306 (1995).
22. T. Niendorf, R. M. Dijkuizen, D. G. Norris, M. van Lookeren Campagne, and K. Nicolay, Biexponential diffusion attenuation in various states of brain tissue: implications for diffusion-weighted imaging, *Magn. Reson. Med.* **36,** 847–857 (1996).
23. T. P. Trouard, N. R. Aiken, and K. A. McGovern, Correlation of extracellular volume fraction and apparent diffusion coefficient in red blood cell

suspensions via DWI and ^{31}P MRS, *Proc. Int. Soc. Magn. Reson. Med.* **5,** 1331 (1997).

24. G. J. Stanisz, J. G. Li, G. A. Wright, and R. M. Henkelman, Water dynamics in human blood via combined measurements of T_2 relaxation and diffusion in the presence of gadolinium, *Magn. Reson. Med.* **39,** 223–233 (1998).
25. K. M. Donahue, D. Burstein, W. J. Manning, and M. L. Gray, Studies of Gd-DTPA relaxivity and proton exchange rates in tissue, *Magn. Reson. Med.* **32,** 66–76 (1994).
26. A. Szafer, J. Zhong, A. W. Anderson, and J. C. Gore, Diffusion weighted imaging in tissues: theoretical models, *NMR Biomed.* **8,** 289–296 (1995).
27. T. Q. Duong, C. S. Springer, C. H. Sotak, G. L. Bretthorst, G. Vetek, I. Palyka, J. J. H. Ackerman, and J. J. Neil, Evaluation of equilibrium transcytolemmal water exchange in intact rat brain, *Proc. Int. Soc. Magn. Reson. Med.* **6,** 530 (1998).
28. M. D. Silva, T. Omae, K. Helmer, F. Li, M. Fisher, and C. Sotak, Separating MR changes of intra- and extracellular water in focal cerebral ischemia in the rat brain, *Proc. Int. Soc. Magn. Reson. Med.* **9,** 457 (2001).